

Article

# Improved Dehydrogenation Performance of Li-B-N-H by Doped NiO

Yipeng Wu, Fen Xu \*, Lixian Sun \*, Yongpeng Xia, Peng Li, Jun Chen, Xia Yang, Fang Yu, Huanzhi Zhang, Hailiang Chu  and Yongjin Zou

Guangxi Key Laboratory of Information Materials, Guangxi Collaborative Innovation Center of Structure and Property for New Energy and Materials, School of Material Science and Engineering, Guilin University of Electronic Technology, Guilin 541004, China; wuyipeng921@163.com (Y.W.); yongpeng\_xia@126.com (Y.X.); lipeng11000@126.com (P.L.); 15737972075@163.com (J.C.); 18078345637@163.com (X.Y.); xyp1510201026@163.com (F.Y.); zhanghuanzhi@guet.edu.cn (H.Z.); chuhailiang@guet.edu.cn (H.C.); zouyongjing518@126.com (Y.Z.)

\* Correspondence: xufen@guet.edu.cn (F.X.); sunlx@guet.edu.cn (L.S.); Tel.: +86-0773-230-3763 (F.X. & L.S.)

Received: 20 March 2018; Accepted: 8 April 2018; Published: 11 April 2018



**Abstract:** In order to improve the dehydrogenation properties of the Li-B-N-H system, a flower-like NiO was successfully synthesized using the hydrothermal method. The effect of the NiO on the dehydrogenation properties of the LiBH<sub>4</sub>-2LiNH<sub>2</sub> system was studied. The results showed that the dehydrogenation properties of the LiBH<sub>4</sub>-2LiMH<sub>2</sub> system were significantly enhanced by doping with NiO. The composite doped with 5 wt. % NiO exhibited optimal hydrogen storage properties. It released about 10.5 wt. % hydrogen below 300 °C, and the onset dehydrogenation temperature was only 90 °C, 110 °C lower than that of LiBH<sub>4</sub>-2LiNH<sub>2</sub>. The isothermal dehydrogenation experiment indicated that the LiBH<sub>4</sub>-2LiNH<sub>2</sub>-5 wt. % NiO composite released 8.8 wt. % hydrogen within 15 min at 150 °C. Structural analysis revealed that the as-prepared NiO was reduced to metallic Ni, which worked as an active catalytic species in the remainder of the dehydrogenation process. The Mass Spectrometer (MS) analyses showed that the doped NiO inhibited the content of NH<sub>3</sub> released in the process of the dehydrogenation of LiBH<sub>4</sub>-2LiNH<sub>2</sub>-NiO.

**Keywords:** lithium borohydride; lithium amide; flower-like NiO; hydrogen storage

## 1. Introduction

In recent years, solid-state complex hydrides bearing lightweight elements or compounds, such as sodium aluminum hydrides, lithium aluminum hydrides, lithium borohydrides, and lithium amides—have been proven to be potential candidates for hydrogen storage [1–3]. Amongst these hydrides, LiBH<sub>4</sub> holds the maximum hydrogen capacity of 18.4 wt. %. However, high thermodynamic stability and poor reversibility limit its practical application as an onboard hydrogen storage medium [4,5].

To overcome these problems, several attempts have been explored, including destabilization [6,7], catalyst additives [8–10], and partial anion–cation substitution [11,12]. For example, Li et al. [13] found that nano-sized Ni could effectively improve the thermodynamic properties of the dehydrogenation of LiBH<sub>4</sub>. With the addition of 25 wt. % Ni, the dehydrogenation peak temperature of LiBH<sub>4</sub> was reduced from 470 to 423 °C, and the dehydrogenation content of LiBH<sub>4</sub> was raised from 4.3 to 10.8 wt. %. Zhang et al. [6] found that nano-sized nickel ferrite (NiFe<sub>2</sub>O<sub>4</sub>) could effectively destabilize LiBH<sub>4</sub>, liberating 10.75 wt. % of hydrogen at 89 °C. As mentioned above, the addition of Ni or nickel-based oxides into LiBH<sub>4</sub> was an efficient way to enhance its dehydrogenation kinetics [14].

In addition, a series of LiBH<sub>4</sub>-metal hydride composites were studied, including LiBH<sub>4</sub>-MgH<sub>2</sub> [15,16], LiBH<sub>4</sub>-CaH<sub>2</sub> [17,18], LiBH<sub>4</sub>-Li<sub>3</sub>AlH<sub>6</sub> [19] and LiBH<sub>4</sub>-Mg<sub>2</sub>NiH<sub>4</sub> [20]. These studies showed that the

dehydrogenation temperature of  $\text{LiBH}_4$  could be reduced, and the dehydrogenation kinetics could be improved. Furthermore, the research revealed that the strong affinity between protic  $\text{H}^+$  and hydridic  $\text{H}^-$  can provide the driving force for hydrogen release [21]. Taking advantage of the interaction between the [B-H] bond and [N-H] bond, the combination of  $\text{LiBH}_4$  and amides was an effective way in which to decrease the dehydrogenation temperature of  $\text{LiBH}_4$ . Pinkerton et al. [22] were the first to dope  $\text{LiNH}_2$  into  $\text{LiBH}_4$ . They found that the  $\text{LiBH}_4$ - $2\text{LiNH}_2$  system released more than 10% hydrogen when heated to 350 °C. The dehydrogenation property was significantly improved compared with the individual  $\text{LiBH}_4$  and  $\text{LiNH}_2$ . However, the dehydrogenation temperature was still high, and the dehydrogenation kinetics were also slow. One of the most effective approaches to improving the dehydrogenation property of  $\text{LiBH}_4$ - $2\text{LiNH}_2$  was to dope transition metals. Pinkerton et al. [23] reported the influence of doped transition metals (Fe, Ni, and Zn) on  $\text{LiBH}_4$ - $2\text{LiNH}_2$ . Recently, Zhang et al. [24] synthesized metallic Ni nanoparticles supported on carbon ( $\text{Ni@C}$ ), and doped 10 wt. %  $\text{Ni@C}$  into  $\text{LiBH}_4$ - $2\text{LiNH}_2$ . The onset dehydrogenation temperature of the sample was 135 °C, and approximately 10 wt. % hydrogen was released within 25 min at 220 °C.

As previously reported, 3D hierarchical flower-like  $\text{MoS}_2$  presented a better catalytic effect on the dehydrogenation of  $\text{LiBH}_4$  compared to that of the powder  $\text{MoS}_2$  [25]. This was attributed to the enlarged interlayer distance of the  $\text{MoS}_2$  nanosheets, 3D architectures, and hierarchical structures. Zhang reported that the as-prepared  $\text{Co}_3\text{O}_4$  exhibited much better catalytic activity for the Li-B-N-H system than the powder sample, the end temperature of dehydrogenation for the majority of the sample with 0.05/3 mol as-prepared  $\text{Co}_3\text{O}_4$  was decreased by 64 °C, compared to the powder sample  $\text{Co}_3\text{O}_4$  [26]. The catalysts with specific structure and size exhibited much better catalytic activity than the powder samples. NiO powders were easy to agglomerate during catalytic reaction, while NiO with a flower-like structure could avoid the agglomeration, and had the advantages of a nanometer effect, as well as a large specific surface area [27]. In this work, we successfully synthesized flower-like NiO via the hydrothermal method, and doped the NiO into the Li-B-N-H system.  $\text{LiBH}_4$ - $2\text{LiNH}_2$ -NiO composite was prepared by ball milling. The influence of NiO on the dehydrogenation performance of the Li-B-N-H system was studied. The results of the experiment showed that doped NiO could enhance the dehydrogenation property and inhibit the release of  $\text{NH}_3$  in the dehydrogenation of the Li-B-N-H system.

## 2. Materials and Methods

### 2.1. Sample Preparation

Commercial chemicals  $\text{LiBH}_4$  95% (Sigma Aldrich, Shanghai, China),  $\text{LiNH}_2$  95% (Alfa Aesar, Shanghai, China), commercial NiO powder (Sinopharm Chemical Reagent Co., Ltd, Shanghai, China) and Ni (J&K, Shanghai, China) were used without further purification. The NiO was prepared using the following hydrothermal method: 5 mmol  $\text{NiCl}_2 \cdot 6\text{H}_2\text{O}$  and 30 mmol NaOH were dissolved (in that order) into 20 mL distilled water to obtain  $\text{NiCl}_2$  solution and NaOH solution. Ethanedi-amine (2 mL) was added to the  $\text{NiCl}_2$  solution while stirring, and a purple solution was obtained. After being stirred for a further 30 min, the above-mentioned NaOH solution was added to the purple solution. Following that, the mixed solution was poured into a 40 mL Teflon-lined autoclave with a stainless steel coat, heated at 140 °C for 4 h, and then left to cool naturally to room temperature. The precipitate was filtered and washed twice with ethanol and distilled water, and was then dried at 80 °C for 4 h under a vacuum. Finally, the dried product was placed in a muffle furnace and heated at 450 °C for 2 h, and the final product was NiO.

The  $\text{LiBH}_4$ - $2\text{LiNH}_2$ - $x$  wt. % NiO composites ( $x = 0, 1, 3, 5, 10$  or 15) were prepared by ball milling (Retsch PM 400, Arzberg, Germany) at 200 rpm under Ar for 2 h. The ball-to-sample weight ratio was 200:1. All samples were handled in a glove box (MABRAUN, Munich, Germany) filled with argon ( $\text{H}_2\text{O} < 0.01$  ppm;  $\text{O}_2 < 0.01$  ppm) in order to avoid  $\text{H}_2\text{O}$  and  $\text{O}_2$  contamination.

## 2.2. Sample Characterization

The dehydrogenation properties of the samples were measured using a pressure composition temperature system (PCT) (pro-2000, Setaram, Lyon, France). The samples were heated from room temperature to 300 °C at a rate of 2 °C/min under N<sub>2</sub> flow. For the isothermal dehydrogenation, the sample was quickly heated to the desired temperature. The gas quantities produced were analyzed using a temperature programmed desorption (TPD, Quantachrome, FL, USA) system equipped with a mass spectrometer (MS, GAM-200, InProcess Instruments, Bremen, Germany). The samples were heated from room temperature to 400 °C at a rate of 5 °C/min by using pure He as the carrier gas.

The phase structures of the samples were characterized using a powder X-ray diffractometer (XRD, Bruker, Karlsruhe, Germany) (Cu K $\alpha$ , 40 KV, 40 mA) over the 2 $\theta$  range of 10–90° in an increment of 0.01°. During the process of XRD measurements, a special sample holder with an airtight mantle was used to protect samples from H<sub>2</sub>O and O<sub>2</sub> contamination. The morphology of the samples was observed using a scanning electron microscope (SEM, S-4800, Hitachi, Tokyo, Japan).

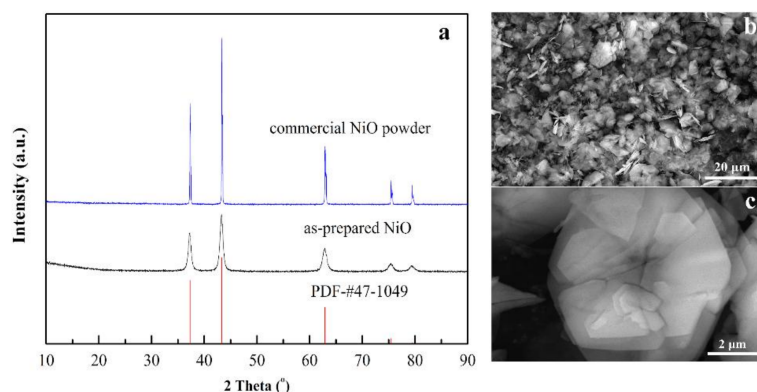
The Fourier-transform infrared spectroscopy (FTIR) analysis was performed using a Nicolet 6700 Fourier-transform infrared spectrometer (Thermo Scientific, Waltham, MA, USA). The powder samples and potassium bromide (KBr) powder were mixed in a 1:100 weight ratio compressed to form a pellet as a test sample. FTIR spectra were recorded from 800 cm<sup>-1</sup> to 4000 cm<sup>-1</sup>.

The nitrogen adsorption and desorption isotherms of the as-prepared NiO and commercial NiO powder were measured at 77 K using nitrogen in a conventional volumetric technique with a Quantachrome Autosorb-iQ2 sorptometer (Quantachrome, FL, USA). Before being measured, the samples were outgassed at 100 °C in a vacuum for 8 h. The specific surface areas of the composites were calculated from the adsorption branch according to the Brunauer–Emmett–Teller (BET) method.

## 3. Results and Discussion

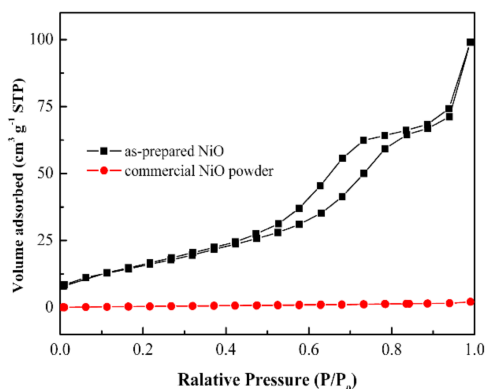
### 3.1. The Phase Structure and Morphology of the Synthesized NiO

Figure 1 shows the XRD pattern and SEM image of the as-prepared NiO sample. From Figure 1a, the diffraction peaks at the 2 $\theta$  = 37.2°, 43.2°, 62.8°, 75.2°, and 79.4° are observed in as-prepared NiO and commercial NiO powder, which can be indexed as (111), (200), (311), (222) lattice planes, in agreement with the standard spectrum (JCPDS, No. 47-1049). In addition, the full width at half maximum of the as-prepared NiO is wider than that of commercial NiO powder, which indicates the smaller crystallite size. Meanwhile, the as-prepared NiO sample is highly purified, as no additional peaks can be observed on the XRD curve. Further SEM observations reveal that the as-prepared NiO sample shows a flower-like structure assembled by numerous nanosheets (see Figure 1b,c).



**Figure 1.** X-ray diffractometer (XRD) pattern (a) and the Scanning Electron Microscope (SEM) images (b) and (c) of the as-synthesized NiO.

In order to further investigate the structure of the as-prepared NiO, the sample nitrogen sorption isotherms are characterized (Figure 2). A distinct hysteresis loop can be observed from 0.4 to 1.0  $P/P_0$  of the as-prepared NiO, indicating the presence of mesopores. However, the commercial NiO powder has almost no pores. The BET specific surface area of the as-prepared NiO is  $59.9 \text{ m}^2 \cdot \text{g}^{-1}$ . The as-prepared NiO maintains a larger specific surface area and mesopores, giving it better catalytic performance than NiO powder for dehydrogenation reactions.



**Figure 2.** Nitrogen sorption isotherms of the as-prepared NiO and commercial NiO powder.

### 3.2. Structural Characteristics of As-Milled Samples

The as-synthesized NiO was introduced into the  $\text{LiBH}_4\text{-}2\text{LiNH}_2$  system by ball milling. Figure 3 shows the XRD patterns and FTIR measurements of the  $\text{LiBH}_4\text{-}2\text{LiNH}_2\text{-}x \text{ wt. \% NiO}$  composites ( $x = 0, 1, 3, 5, 10, \text{ or } 15$ ). It can be seen from Figure 3a that the  $\text{LiBH}_4\text{-}2\text{LiNH}_2$  sample consists of the  $\text{Li}_4\text{BN}_3\text{H}_{10}$  primary phase ( $\alpha$  phase) and minor  $\text{Li}_2\text{BNH}_6$  phase ( $\beta$  phase) [28]. After doping NiO, the  $\text{Li}_4\text{BN}_3\text{H}_{10}$  phase still dominates the XRD profile, but the diffraction pattern of  $\text{Li}_2\text{BNH}_6$  phase is not observed, indicating that the addition of NiO facilitates the formation of the  $\text{Li}_4\text{BN}_3\text{H}_{10}$  phase. However, by increasing the content of NiO, the  $\text{Li}_4\text{BN}_3\text{H}_{10}$  phase is gradually weakened. As the content of NiO increases to 5 wt. %, the characteristic diffraction peaks of NiO are clearly visible and are gradually enhanced by increasing the NiO content. Further FTIR measurements (see Figure 3b) indicate the characteristic B-H stretching modes ( $2376$  and  $2225 \text{ cm}^{-1}$ ),  $\text{BH}_2$  deformation bands ( $1125$  and  $1077 \text{ cm}^{-1}$ ), and N-H stretches ( $3375$  and  $3245 \text{ cm}^{-1}$ ) [29] in FTIR curves, all of which confirm the presence of the  $\text{Li}_4\text{BN}_3\text{H}_{10}$  phase.

Therefore, we conclude that the  $\text{Li}_4\text{BN}_3\text{H}_{10}$  phase is formed by the reaction between  $\text{LiBH}_4$  and  $\text{LiNH}_2$  during the ball milling process of the  $\text{LiBH}_4\text{-}2\text{LiNH}_2\text{-}x \text{ wt. \% NiO}$  mixture. The NiO remains nearly unchanged.

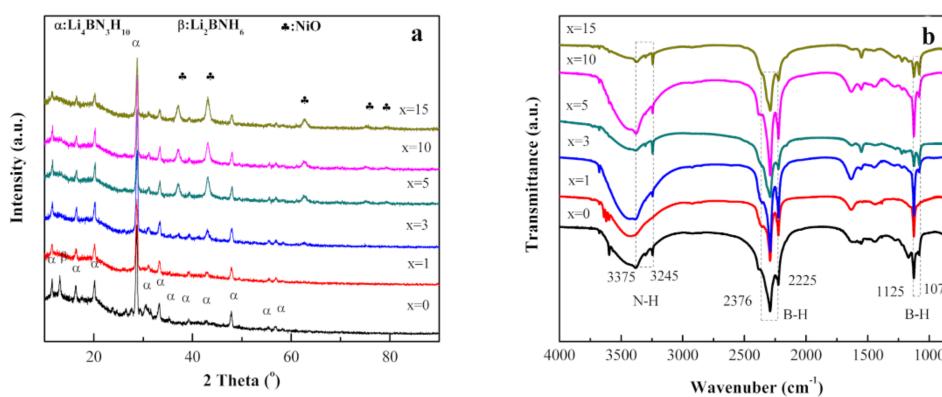


**Figure 3.** XRD patterns (a) and FTIR spectra (b) of the  $\text{LiBH}_4\text{-}2\text{LiNH}_2\text{-}x \text{ wt. \% NiO}$ .

### 3.3. Dehydrogenation Behaviors of Doped NiO Samples

The dehydrogenation behaviors of doped NiO samples were evaluated by PCT. Figure 4 presents the curves of hydrogen-releasing  $\text{LiBH}_4\text{-2LiNH}_2\text{-}x$  wt. % NiO samples. From Figure 4, it is clear that doped NiO significantly improves the dehydrogenation properties of the  $\text{LiBH}_4\text{-2LiNH}_2$  system. After adding 1 wt. % NiO, the onset dehydrogenation temperature was reduced to 140 °C. The onset dehydrogenation temperature was reduced by 60 °C in contrast with the pristine  $\text{LiBH}_4\text{-2LiNH}_2$  sample. With the content of NiO increasing, the onset dehydrogenation temperature gradually decreases. However, as the content of NiO reaches 10 wt. %, the amount of hydrogen released decreases too. Therefore, the doped 5 wt. % NiO sample has the best dehydrogenation performance—the starting dehydrogenation temperature is only 90 °C, and decreases by about 110 °C compared with the pristine  $\text{LiBH}_4\text{-2LiNH}_2$  sample, and approximately 10.5 wt. % of hydrogen is liberated when heated to 300 °C. Moreover, as doped NiO is greater than 5 wt. %, the dehydrogenation process is divided into two stages, occurring at 90–140 °C and 140–300 °C respectively, meaning that the doped NiO is able to change the dehydrogenation pathway, as has been previously reported [28]. Furthermore, the as-prepared NiO shows much better catalytic activity than that of the powder sample. Results demonstrate that the onset dehydrogenation temperature of the 5 wt. % as-prepared NiO sample is 55 °C lower than that of the 5 wt. % NiO powder-added  $\text{LiBH}_4\text{-2LiNH}_2$  sample (Figure 5). This is possibly due to its high specific surface area and nanometer effect [30].

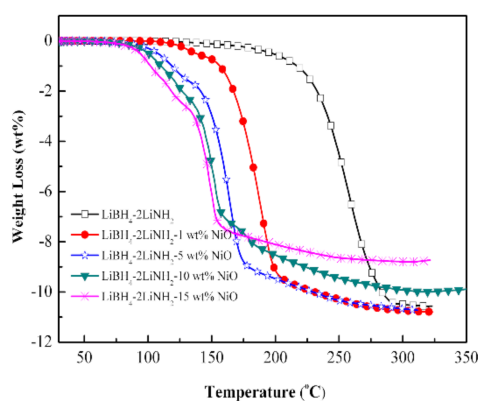


Figure 4. PCT curves of the  $\text{LiBH}_4\text{-2LiNH}_2\text{-}x$  wt. % NiO samples.

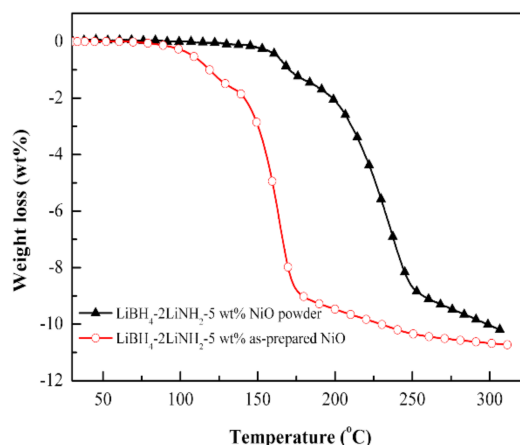
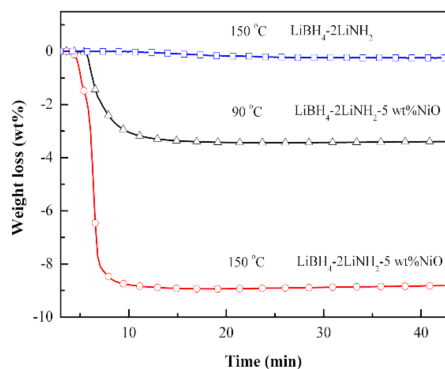


Figure 5. PCT curves of 5 wt. % as-prepared NiO and 5 wt. % NiO powder-added  $\text{LiBH}_4\text{-2LiNH}_2$  samples.

For the  $\text{LiBH}_4\text{-2LiNH}_2\text{-5 wt. % NiO}$  sample, the isothermal dehydrogenation property has been studied at 90 °C and 150 °C respectively, as shown in Figure 6. From Figure 6, we can see that the

isothermal dehydrogenation property of the  $\text{LiBH}_4\text{-2LiNH}_2\text{-NiO}$  is significantly enhanced. Even at a temperature as low as  $90^\circ\text{C}$ , the  $\text{LiBH}_4\text{-2LiNH}_2\text{-5 wt. \% NiO}$  composites release 3.1 wt. % of hydrogen in 15 min. When heated to  $150^\circ\text{C}$ , the  $\text{LiBH}_4\text{-2LiNH}_2\text{-5 wt. \% NiO}$  sample releases 8.8 wt. % hydrogen in 15 min. For the pristine  $\text{LiBH}_4\text{-2LiNH}_2$  sample, almost no hydrogen desorption is detected under the same conditions. These results show that  $\text{LiBH}_4\text{-2LiNH}_2\text{-NiO}$  have better dehydrogenation kinetics than the pristine  $\text{LiBH}_4\text{-2LiNH}_2$ .



**Figure 6.** Isothermal dehydrogenation curves of the  $\text{LiBH}_4\text{-2LiNH}_2\text{-NiO}$ .

### 3.4. MS Analysis

Figure 7 presents the TPD-MS curves of the  $\text{LiBH}_4\text{-2LiNH}_2\text{-}x$  wt. % NiO composites. As shown in Figure 7a, one strong dehydrogenation peak at  $330^\circ\text{C}$  is observed in the TPD-MS curve of the pristine  $\text{LiBH}_4\text{-2LiNH}_2$  system, which indicates a one-step reaction of dehydrogenation corresponding to the decomposition of the  $\text{Li}_4\text{BN}_3\text{H}_{10}$ . After doping NiO, two dehydrogenation peaks appear in their TPD-MS curves, and these peaks appear sooner than in the case of the  $\text{LiBH}_4\text{-2LiNH}_2$  system. Because the first peak is very small, as doped NiO is 1 wt. %, its PCT curve only shows one stage (see Figure 4). This result is further evidence that the doped NiO can change the dehydrogenation pathway.

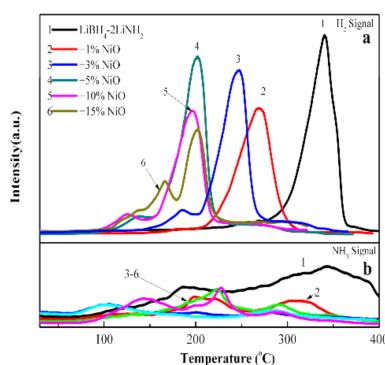


**Figure 7.** MS- $\text{H}_2$  signals (a) and  $\text{NH}_3$  signals (b) of the as-milled  $\text{LiBH}_4\text{-2LiNH}_2\text{-}x$  wt. % NiO.

According to Figure 7b, the  $\text{NH}_3$  by-product, which originates from the decomposition of the  $\text{NH}_2$  group in the  $\text{Li}_3\text{BN}_2\text{H}_8$ , as previously reported [31], is still present during the dehydrogenation process, however its amounts are obviously reduced. It follows that doped NiO inhibits the release of  $\text{NH}_3$  in the dehydrogenation process.

### 3.5. Dehydrogenation Mechanism of the $\text{LiBH}_4\text{-2LiNH}_2\text{-5 wt. \% NiO}$

To clarify the chemical events occurring during the dehydrogenation process, XRD and FTIR examinations of  $\text{LiBH}_4\text{-2LiNH}_2\text{-5 wt. \% NiO}$  composite at different dehydrogenation stages were

carried out, and their results are summarized in Figure 8. As shown in Figure 8a, the  $\text{LiBH}_4\text{-}2\text{LiNH}_2\text{-}5$  wt. % NiO composite is mainly composed of two phases—that is, the  $\text{Li}_4\text{BN}_3\text{H}_{10}$  [30] phase and the NiO phase. After dehydrogenation at  $90^\circ\text{C}$ , it can be seen from the XRD pattern that the  $\text{Li}_4\text{BN}_3\text{H}_{10}$  phase is still the primary phase; the characteristic peaks of NiO have disappeared, and a weaker peak of Ni appears at  $44.5^\circ$ , indicating that the NiO is reduced to the metallic Ni by the dehydrogenation process. According to its FTIR spectrum, the absorption peaks of the B-H stretching modes of the  $\text{BH}_4$  group, the  $\text{BH}_2$  deformation bands, and N-H stretches can still be observed, but clearly decreased. Meanwhile, a new absorption peak of the B-N vibration is observed from  $1700\text{ cm}^{-1}$  to  $1750\text{ cm}^{-1}$ , which indicates the formation of  $\text{Li}_3\text{BN}_2$  [32]. After dehydrogenation at  $150^\circ\text{C}$ , the absorption peak of the B-N vibration becomes strong, indicating that the content of the compound containing a B-N bond is increasing. After full dehydrogenation at  $300^\circ\text{C}$ , only the typical reflections of the  $\text{Li}_3\text{BN}_2$  and Ni can be observed. Further FTIR analyses indicate that only the absorption peaks of the B-N bond are observed. Therefore, we speculate that the solid product is  $\text{Li}_3\text{BN}_2$ , after full dehydrogenation at  $300^\circ\text{C}$ .

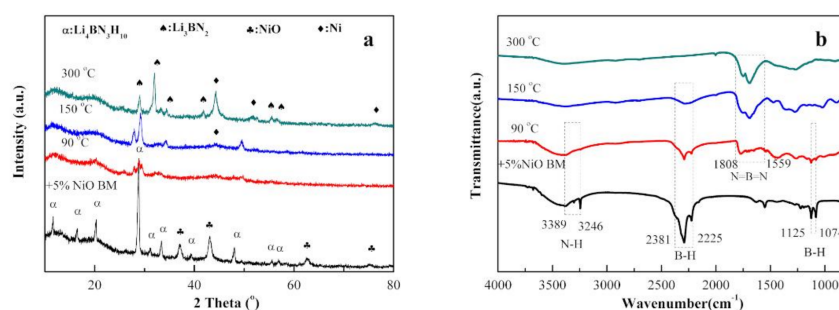


**Figure 8.** XRD patterns (a) and FTIR spectra (b) of the dehydrogenated  $\text{LiBH}_4\text{-}2\text{LiNH}_2\text{-}5$  wt. % NiO.

The obtained results demonstrate that the NiO is firstly reduced to Ni during the dehydrogenation process of  $\text{LiBH}_4\text{-}2\text{LiNH}_2\text{-NiO}$ . The newly formed metallic Ni works as an active catalytic species to reduce the dehydrogenation temperature of the  $\text{LiBH}_4\text{-}2\text{LiNH}_2\text{-}5$  wt. % NiO composite. Similar results have also been observed for a directly Ni-doped Li-B-N-H system. The metallic Ni has high catalytic activity, and the B-N bonds can be easily created on the surface of metallic Ni [33]. As shown in Figure 9, the dehydrogenation properties of the Li-B-N-H system are improved by the doped NiO or metallic Ni. However, the onset dehydrogenation temperature of doped NiO is  $85^\circ\text{C}$  lower than that of doped Ni, although their catalytic species are both Ni. This illustrates that while the effect of doped NiO is similar to that of doped Ni, the in situ produced Ni has better catalytic performance than that of the directly doped metallic Ni.

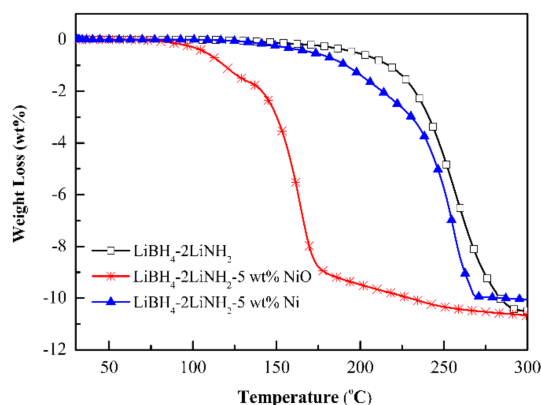


**Figure 9.** Non-isothermal dehydrogenation curves of the  $\text{LiBH}_4\text{-}2\text{LiNH}_2$  with different additives.

#### 4. Conclusions

In this work, a flower-like NiO additive has been synthesized via a hydrothermal process, and doped into the  $\text{LiBH}_4\text{-2LiNH}_2$  system in order to improve the hydrogen storage properties. The results indicated that by doping a small amount of NiO, the onset temperature of the  $\text{LiBH}_4\text{-2LiNH}_2$  system can be reduced significantly, and the dehydrogenation kinetics can be enhanced. The  $\text{LiBH}_4\text{-2LiNH}_2\text{-5 wt. \% NiO}$  composite exhibited optimal hydrogen storage properties, with the sample releasing approximately 10.5 wt. % hydrogen below 300 °C. The onset dehydrogenation temperature of the composite with an additive was only 90 °C, which was 110 °C lower than that of  $\text{LiBH}_4\text{-2LiNH}_2$ . The isothermal dehydrogenation indicated that the  $\text{LiBH}_4\text{-2LiNH}_2\text{-5 wt. \% NiO}$  released 8.8 wt. % hydrogen within 15 min at 150 °C. Moreover, the  $\text{LiBH}_4\text{-2LiNH}_2\text{-5 wt. \% NiO}$  exhibited a two-stage dehydrogenation process, indicating that the dehydrogenation pathway had changed. The NiO was reduced to Ni at the first stage of the dehydrogenation process, which worked as an active catalytic species for the remainder of the dehydrogenation process. The MS analyses showed that doping NiO can inhibit the release of  $\text{NH}_3$  in the process of dehydrogenation.

**Acknowledgments:** This work was supported by the National Natural Science Foundation of China (No. 51361005, U1501242, 51671062 and 51371060), by Guangxi Collaborative Innovation Centre of Structure and Property for New Energy and Material (2012GXNSFGA06002), and by the Guangxi Key Laboratory of Information Laboratory Foundation (No. 161002-Z and 161002-K).

**Author Contributions:** Yipeng Wu contributed the central idea, analysed most of the data, performed the mass experiments, made the chart, and wrote the manuscript; Fen Xu and Lixian Sun contributed to refine the ideas, analyse the data and guide the writing of the manuscript; Yongpeng Xia analysed part of the data and revised the chart; Peng Li, Xia Yang and Jun Chen retrieved the references, collected the data and carried out part of the experiments; Fang Yu, Huanzhi Zhang, Hailiang Chu and Yongjin Zou analysed part of the data and revised the English language and style. All authors read and approved the final manuscript, and agreed to be accountable for all aspects of the work.

**Conflicts of Interest:** The authors declare no conflict of interest.

#### References

1. Züttel, A.; Rentsch, S.; Fischer, P.; Wenger, P.; Sudan, P.; Mauron, P. Hydrogen storage properties of  $\text{LiBH}_4$ . *J. Alloy Compd.* **2003**, *356*, 515–520. [[CrossRef](#)]
2. Hu, Y.H. Novel hydrogen storage systems and materials. *Int. J. Energy Res.* **2013**, *37*, 683–685. [[CrossRef](#)]
3. Zhang, L.; Chen, L.; Fan, X.; Xiao, X.; Zheng, J.; Huang, X. Enhanced hydrogen storage properties of  $\text{MgH}_2$  with numerous hydrogen diffusion channels provided by  $\text{Na}_2\text{Ti}_3\text{O}_7$  nanotubes. *J. Mater. Chem. A* **2017**, *5*, 6178–6185. [[CrossRef](#)]
4. Khafidz, N.Z.A.K.; Yaakob, Z.; Lim, K.L.; Timmiati, S.N. The kinetics of lightweight solid-state hydrogen storage materials: A review. *Int. J. Hydrogen Energy* **2016**, *41*, 13131–13151.
5. Moller, K.T.; Fogh, A.S.; Paskevicius, M.; Skibsted, J.; Jensen, T.R. Metal borohydride formation from aluminium boride and metal hydrides. *Phys. Chem.* **2016**, *18*, 27545–27553. [[CrossRef](#)] [[PubMed](#)]
6. Zhang, J.; Li, P.; Wan, Q.; Zhai, F.Q.; Volinsky, A.A.; Qu, X.H. Superior destabilization effects of  $\text{LiBH}_4$  with the addition of nano-sized nickel ferrite  $\text{NiFe}_2\text{O}_4$ . *RSC Adv.* **2015**, *5*, 81212–81219. [[CrossRef](#)]
7. Gosalawit-Utke, R.; Meethom, S.; Pistidda, C.; Milanese, C.; Laipple, D.; Saisopa, T. Destabilization of  $\text{LiBH}_4$  by nanoconfinement in PMMA-co-BM polymer matrix for reversible hydrogen storage. *Int. J. Hydrogen Energy* **2014**, *39*, 5019–5029. [[CrossRef](#)]
8. Liu, X.; Langmi, H.W.; Beattie, S.D.; Azenwi, F.F.; McGrady, G.S.; Jensen, C.M. Ti-Doped  $\text{LiAlH}_4$  for Hydrogen Storage: Synthesis, Catalyst Loading and Cycling Performance. *J. Am. Chem. Soc.* **2011**, *133*, 15593–15597. [[CrossRef](#)] [[PubMed](#)]
9. Xu, J.; Meng, R.R.; Cao, J.Y.; Gu, X.F.; Song, W.L.; Qi, Z.Q. Graphene-supported Pd catalysts for reversible hydrogen storage in  $\text{LiBH}_4$ . *J. Alloys Compd.* **2013**, *564*, 84–90. [[CrossRef](#)]
10. Wang, H.X.; Zhou, L.M.; Han, M.; Tao, Z.L.; Cheng, F.Y.; Chen, J. CuCo nanoparticles supported on hierarchically porous carbon as catalysts for hydrolysis of ammonia borane. *J. Alloys Compd.* **2015**, *651*, 382–388. [[CrossRef](#)]

11. Shao, J.; Xiao, X.Z.; Chen, L.X.; Fan, X.L.; Han, L.Y.; Li, S.Q. Enhanced hydriding-dehydriding performance of a 2LiH-MgB<sub>2</sub> composite by the catalytic effects of Ni-B nanoparticles. *J. Mater. Chem. A* **2013**, *1*, 10184–10192. [[CrossRef](#)]
12. Yang, Z.; Grant, D.M.; Wang, P.; Walker, G.S. The effect of complex halides and binary halides on hydrogen release for the 2LiBH<sub>4</sub>:1MgH<sub>2</sub> system. *Faraday Discuss.* **2011**, *151*, 133–141. [[CrossRef](#)] [[PubMed](#)]
13. Li, H.W.; Yan, Y.G.; Akiba, E.; Orimo, S.I. Improved Dehydrogenation and Rehydrogenation Properties of LiBH<sub>4</sub> by Nanosized Ni Addition. *Mater. Trans.* **2014**, *8*, 1134–1137. [[CrossRef](#)]
14. Chen, S.; Miao, C.X.; Luo, Y.; Zhou, G.L.; Xiong, K.; Jiao, Z.J.; Zhang, X.M. Study of catalytic hydrodeoxygenation performance of Ni catalysts: Effects of prepared method. *Renew. Energy* **2017**, *115*, 1109–1117. [[CrossRef](#)]
15. Vajo, J.J.; Skeith, S.L.; Mertens, F. Reversible storage of hydrogen in destabilized LiBH<sub>4</sub>. *J. Phys. Chem. B* **2005**, *109*, 3719–3722. [[CrossRef](#)] [[PubMed](#)]
16. Pinkerton, F.E.; Meyer, M.S.; Meisner, G.P.; Balogh, M.P.; Vajo, J.J. Phase Boundaries and Reversibility of LiBH<sub>4</sub>/MgH<sub>2</sub> Hydrogen Storage Material. *J. Phys. Chem. C* **2007**, *111*, 12881–12885. [[CrossRef](#)]
17. Lim, J.H.; Shim, J.H.; Lee, Y.S.; Suh, J.Y.; Cho, Y.W. Rehydrogenation and cycle studies of LiBH<sub>4</sub>-CaH<sub>2</sub> composite. *Int. J. Hydrogen Energy* **2010**, *13*, 6578–6582. [[CrossRef](#)]
18. Lbikunle, A.; Goudy, A.J.; Yang, H. Hydrogen storage in a CaH<sub>2</sub>/LiBH<sub>4</sub> destabilized metal hydride system. *J. Alloys Compd.* **2009**, *475*, 110–115. [[CrossRef](#)]
19. Wu, X.C.; Wang, X.H.; Cao, G.Z.; Li, S.Q.; Ge, H.W.; Chen, L.X.; Yan, M. Hydrogen storage properties of LiBH<sub>4</sub>-Li<sub>3</sub>AlH<sub>6</sub> composites. *J. Alloys Compd.* **2012**, *517*, 127–131. [[CrossRef](#)]
20. Javadian, P.; Zlotea, C.; Ghimbeu, C.M.; Jenson, T.R. Hydrogen storage properties of nanoconfined LiBH<sub>4</sub>-Mg<sub>2</sub>NiH<sub>4</sub> reactive hydride composites. *J. Phys. Chem. C* **2015**, *119*, 5819–5826. [[CrossRef](#)]
21. Chen, P.; Xiong, Z.T.; Luo, J.Z.; Lin, J.Y.; Tan, K.L. Interaction of hydrogen with metal nitrides and imides. *Nature* **2002**, *420*, 302–304. [[CrossRef](#)] [[PubMed](#)]
22. Pinkerton, F.E.; Meyer, M.S.; Meisner, G.P.; Balogh, M.P.; Kundrat, M.D. Hydrogen desorption exceeding ten weight percent from the new quaternary hydride Li<sub>3</sub>BN<sub>2</sub>H<sub>8</sub>. *J. Phys. Chem. B* **2005**, *9*, 6–8. [[CrossRef](#)] [[PubMed](#)]
23. Pinkerton, F.E.; Meyer, M.S.; Meisner, G.P.; Balogh, M.P. Improved hydrogen release from LiB<sub>0.33</sub>N<sub>0.67</sub>H<sub>2.67</sub> with metal additives: Ni, Fe, and Zn. *J. Alloys Compd.* **2007**, *433*, 282–291. [[CrossRef](#)]
24. Zhang, Y.; Liu, Y.F.; Zhang, X.; Li, Y.; Gao, M.X.; Pan, H.G. Synthesis of a Nanosized Carbon-Supported Ni Composite and Its Remarkable Catalysis for Hydrogen Desorption from the LiBH<sub>4</sub>-2LiNH<sub>2</sub> System. *J. Phys. Chem. C* **2015**, *119*, 24760–24768. [[CrossRef](#)]
25. Zhao, Y.; Liu, Y.C.; Liu, H.Q.; Kang, H.Y.; Cao, K.Z.; Wang, Q.H.; Zhang, C.L.; Wang, Y.J. Improved dehydrogenation performance of LiBH<sub>4</sub> by 3D hierarchical flower-like MoS<sub>2</sub> spheres additives. *J. Power Sources* **2015**, *300*, 358–364. [[CrossRef](#)]
26. Li, Y.; Zhang, Y.; Gao, M.X.; Pan, H.G.; Liu, Y.F. Preparation and catalytic effect of porous Co<sub>3</sub>O<sub>4</sub> on the hydrogen storage properties of a Li-B-N-H system. *Prog. Nat. Sci. Mater. Int.* **2017**, *27*, 132–138. [[CrossRef](#)]
27. Zhao, B.; Ke, X.; Bao, J.H.; Wang, C.L.; Dong, L.; Chen, W.Y.; Chen, H.L. Synthesis of flower-like NiO and effects of morphology on its catalytic properties. *J. Phys. Chem. C* **2010**, *113*, 14440–14447. [[CrossRef](#)]
28. Zhang, Y.; Liu, Y.F.; Liu, T.; Gao, M.X.; Pan, H.G. Remarkable decrease in dehydrogenation temperature of Li-B-N-H hydrogen storage system with CoO additive. *Int. J. Hydrogen Energy* **2013**, *38*, 13318–13327. [[CrossRef](#)]
29. Meisner, G.P.; Scullin, M.L.; Balogh, M.P.; Pinkerton, F.E.; Meyer, M.S. Hydrogen release from mixtures of lithium borohydride and lithium amide: A phase diagram study. *J. Phys. Chem. B* **2006**, *110*, 4186–4192. [[CrossRef](#)] [[PubMed](#)]
30. Gao, Q.; Zeng, W.; Miao, R.Y. Synthesis of multifarious hierarchical flower-like NiO and their gas-sensing properties. *J. Mater. Sci. Mater. Electron.* **2016**, *27*, 9410–9416. [[CrossRef](#)]
31. Chater, P.A.; Adeson, P.A.; Prendergast, J.W.; Walton, A.; Vicky, S.J.; David, B.; David, W.; Johnson, S.R.; Edwards, J.J. Synthesis and characterization of amide-borohydrides: New complex light hydrides for potential hydrogen storage. *J. Alloys Compd.* **2007**, *446*, 350–354. [[CrossRef](#)]

32. Liu, Y.F.; Luo, K.; Zhou, Y.F.; Gao, M.X.; Pan, H.G. Diffusion controlled hydrogen desorption reaction for the  $\text{LiBH}_4/2\text{LiNH}_2$  system. *J. Alloys Compd.* **2009**, *481*, 473–479. [[CrossRef](#)]
33. Xu, Q.; Chandra, M. Catalytic activities of non-noble metals for hydrogen generation from aqueous ammonia-borane at room temperature. *J. Power Sources* **2006**, *163*, 364–370. [[CrossRef](#)]



© 2018 by the authors. Licensee MDPI, Basel, Switzerland. This article is an open access article distributed under the terms and conditions of the Creative Commons Attribution (CC BY) license (<http://creativecommons.org/licenses/by/4.0/>).